Plant Oil Fillers Toughened Poly(3-hydroxybutyrate) Green Biocomposites

Joseph Kinyanjui Muiruri[1, §], Jayven Chee Chuan Yeo[2, §], Hong Run[3,§], Ting Ting Lin[2], Xunan Hou[3], Vijayakumar Raveenkumar[2], Boo Yi Jian[2], Warintorn Thitsartarn[2], Chaobin He[2,3,], Zibiao Li[1,2,3,*]*

[1] Institute of Sustainability for Chemicals, Energy and Environment (ISCE[2]), Agency for Science, Technology and Research (A*STAR), 1 Pesek Road, Jurong Island, Singapore 627833, Republic of Singapore

[2] Institute of Materials Research and Engineering (IMRE), Agency for Science, Technology and Research (A*STAR), 2 Fusionopolis Way, Innovis #08-03, Singapore 138634, Republic of Singapore

[3] Department of Materials Science and Engineering, National University of Singapore, 9 Engineering Drive 1, Singapore 117576

§ *The authors contribute equally to this manuscript.*

Correspondence to:

Li Zibiao, email: lizb@imre.a-star.edu.sg (Z.Li)

He Chaobin, e-mail: msehc@nus.edu.sg (C. He)

Abstract

Poly(3-hydroxybutyrate) (PHB) faces a significant challenge of intrinsic brittleness, thus limiting its widespread applicability. This challenge can be surmounted by incorporating various nanofillers into the PHB matrix to tune the mechanical performance. However, many of these fillers are produced using unsustainable, non-environmentally friendly methods. Herein, we employed a green process to develop castor-oil-based fillers, CO-*g*-DLA, and CO-P(CL-*co*-DLA)-PDLA (CO-*r*-DLA), for the toughening of the PHB matrix. Impressively, the addition of 20% of these fillers increases the elongation at the break by 13-fold through forming elongated fibril structures and enhanced interfacial interactions between fillers and the matrix, accompanying by a substantial reduction on the PHB's brittleness through shear yielding and fibrillation. These are confirmed by Small-Angle X-ray Scattering (SAXS) results, showing significant copolymer-induced microstructural changes in the matrix. The biodegradable PHB biocomposite developed in this study offers a promising green alternative to conventional plastics, especially in sustainable packaging.

Keywords: Polyol, Poly(3-hydroxybutyrate), Solvent-free, Fillers, Mechanical properties

Introduction

Global pollution, primarily caused by plastics like polypropylene, polyethylene, and PVC, has become a significant concern.[1, 2] 70% of all plastic produced ends up in landfills, causing potential impacts such as carbon and nutrient cycle changes, habitat changes, biological impacts on endangered species, ecotoxicity, and societal effects.[1, 3] Researchers are exploring safer alternatives to synthetic plastics, such as biodegradable polymers like PLA, PCL, PHAs, and starch. These biodegradable, renewable, and low-carbon polymers can be broken down by microorganisms in controlled environments, reducing plastic waste and promoting a sustainable future.[4, 5]

PHAs, naturally occurring biopolymers accumulated by microorganisms in the form of granules with diameters of 200–700 nm, are expected to reach a market size of USD 27.9 billion by 2025 due to their promising features and the push for green materials. Approved by the FDA for food-contact applications, PHAs are biodegradable and compostable in all mediums, making them suitable to curb marine litter problems. In the PHA family, poly-β-hydroxybutyrate (PHB) is the most studied since its discovery in the 1920s.[6] PHB has certain advantages such as biocompatibility, thermoformability, and mechanical strength, which makes it potential for applications in sustainable areas of packaging, biomedicine, energy, agriculture, and animal feeds.[7, 8]

However, unmodified PHB is limited in industrial applications due to significant defects, such as poor mechanical properties, high brittleness, high crystallinity, and low thermal stability.[7, 9] High brittleness is one of the biggest challenges, making it unsuitable for many applications and products that demand high flexibility and toughness.[9, 10] In addition, PHB is susceptible to

hydrolysis and photolysis, which may limit the shelf life of PHB-based products. To circumvent these challenges, various modification strategies, such as blending with other polymers or copolymers[11, 12], additives such as plasticizers[13, 14], nanofillers[15, 16], cross-linkers[17] etc., have been proposed over the years.[18, 19] Another alternative approach of improving the mechanical properties of PHB is copolymerization with different monomers. In this approach, copolymerization with different monomers produces medium chain length (M-CL) PHAs that are not brittle but has improved mechanical properties.[10, 20] The MCL-PHAs been reported in literature include poly(3-hydroxybutyrate-co-4-hydroxybutyrate) (PHB-4HB), copolymers of poly(3-hydroxybutyrate-co-3-hydroxyhexanoate) (PHB-HHx), and poly(3-hydroxyoctanoate) (PHO).[10] For instance, the mechanical properties of poly(4HB) especially its ductile nature (elongation at break ~1000%) makes it suitable as a comonomer of PHB to produce toughened polymers by copolymerization.[21] This copolymerization approach results in PHB copolymers displayed lower crystallinity resulting in reduced brittleness.

For instance, Yeo *et al.*[11] blended synthesized PHB-rubber fillers with PLA to obtain highly extensive composites suitable for shape memory sensors.[22] Their work reported that PHB-based filler (PHB-*di*-rub) had a synergetic effect as an effective nucleator and toughening modifier for the PLA matrix. Notably, at low content of only 5% (1.5 wt.% PHB content), the strain at break increased to 300%, whereas 10% of PHB-*di*-rub (3 wt.% PHB content) resulted in 680% strain, with uncompromised strength and stiffness. Similar works revealed good results from synthesized PHB fillers in PLA.[22-24] In recent work, Chen *et al.*[12], blended PLA with low content of poly[(*R*)-3-hydroxybutyrate-*co*-4-hydroxybutyrate] (P3HB4HB ≤8 wt.%) to improve the heat resistance of the resultant spun fibers effectively. The authors reported a

significant drop in boiling water shrinkage of about 90% compared with ca. 80% for neat PLA spun fibers. They ascribed the improved heat resistance of the PLA/PHB blend fibers to the increased mobility and orientation of the PLA chains aided by the presence of PHB. Subsequently, Etxeberria *et al.* [25] studied the effect of tributyl citrate (TBC) as a plasticizer for PLA and PHB toughening. In their work, the TBC plasticizer effectively reduced the glass transition temperature of PLA and PHB. Even with the addition of up to 20% TBC, the barrier properties of PHB were unaffected. On the other hand, PLA was found to change in properties ascribed to many factors, including an apparent increase in free volume fraction. Other notable plasticizers for PHAs include levulinic acid[13], tributyrin[26], olive oil, and carvacrol[27] etc.

On the other hand, bioresources such as clay[15], cellulose[16, 28], natural oils[29] etc., are valued fillers that could be harnessed to enhance the properties performance of biopolymers including PHB. In this respect, natural oils from both plant and animal sources are abundant in nature, making them a viable alternative chemical feedstock among bioresources.[30] Typically, castor oil and its derivatives, made up mostly of ricinoleic acid with a secondary hydroxyl group and glycerol has been used to make resins and other numerous applications.[31] For instance, Hosoda *et al*.[32] prepared 3-arm branched PLA by ring opening L-lactide with castor oil and tin octanoate catalyst. The resultant branched polymer was an effective heterogenous nucleator for PHBV, improving the crystallization process. This improvement was attributed to the induced phase separation, which remarkably suppressed the formation of large spherulites of PHBV, thus enhancing the crystallization rate. Interestingly, the authors did not report the mechanical properties of the modified PHBV. In other works, castor oil was used as a polyol for polyurethanes, widely used in the automotive, building, and furniture industries. [33-35] There

have also been reports of functional polymers derived from castor oil and derivatives of ricinoleic acid.[36] For instance, lactic acid and castor oil utilizing phosphoric acid as a catalyst as well as the preparation and thermal characteristics of the copolyester of lactic acid and ricinoleic acid[37-39]

In this work, we report on solvent-free synthesis of a branched poly(D-lactic acid) material employing ring-opening polymerization (ROP) to graft a random sequence of D-lactide and caprolactone from castor oil, and the impact of this filler on the toughening of PHB. Adding only 10% and 20% CO-P(*CL-co-DLA*)-DLA fillers (herein referred to CO-*r*-DLA) increased the flexibility by about 3-fold and 13-fold, respectively, compared to pure PHB. Conversely, without the rubber segment, 10% CO-*g*-DLA did not significantly enhance PHB's flexibility (ε = 12.21%), but 20% CO-*g*-DLA enhanced the strain at break by 13-fold. FESEM and SAXS analysis confirm a change in morphology and microstructure occasioned by filler type and the content. Shear yielding and fibrillation are the proposed toughening mechanisms for PHB filled with castor-oil-based fillers. Overall, the modified PHB is a promising sustainable material with potential use in various applications, particularly in sustainable packaging.

EXPERIMENTAL

Materials and Methods

Castor oil (Sigma-Aldrich), ε-caprolactone monomer (97.0%, Sigma-Aldrich), and tin(II) octoate ($Sn(Oct)_2$) (92.5-100.0%), Sigma-Aldrich) catalyst, Chloroform (99.0%, TCI chemicals, Japan), Ethanol (≥99.8%, Sigma-Aldrich), PHB (ENMAT Y3000) (M_n = 1.62 × 10^5 Da) was purchased from TianAn Technologies; Purasorb D® (D-lactide) monomer was

sourced from Corbion Purac. Chloroform Ethanol All other chemicals were used as received.

Solventless synthesis of castor oil-based fillers.

The ROP method was employed to create castor oil-based fillers. Prior to usage, all required glassware was first dried in an oven. Typically, for CO-P(CL-*co*-DLA)-PDLA or CO-*r*-DLA, the flask was then filled with a monomer's mixture of ε-caprolactone (10.273 g, 90 mmol), D-lactide (5.186 g, 35.98 mmol), and castor oil (CO) (0.093 g, 0.1 mmol), which was used as an initiator. After multiple nitrogen gas purges, 0.3 mmol of the tin(II) octoate ($Sn(Oct)_2$) catalyst was added and, the mixture was gently stirred in a silicon oil bath at 130 °C overnight. Sequentially, D-lactide (5.186 g, 35.98 mmol) was added and reacted for an additional 24 h. The resulting polymeric product was then dispersed in $CHCl_3$, re-precipitated into surplus methanol, separated by filtering, and dried under vacuum. The same procedure was applied for CO-*g*-DLA, except that only the D-lactide monomer was used in the ROP.

Fabrication of PHB/CO-*g*-DLA and PHB/CO-*r*-DLA green biocomposites.

To fabricate the samples, a suitable quantity of PHB powder and either CO-*r*-DLA or CO-*g*-DLA were dissolved in 100 mL of chloroform at 70 °C. Following complete dissolution, the mixture was poured onto a 15-cm crystallizing dish and allowed to evaporate for about 3 days. The resulting uniform films were then vacuum-dried at 60 °C overnight and kept in a dry box for further characterization. Likewise, neat PHB is prepared by the solvent casting method.

Characterizations

Molecular structure and molecular weight determination ^{1}H NMR analysis was performed by Bruker 400 MHz spectrometer at 64 scans using $CDCl_3$ as a solvent and internal standard (δ = 7.26 ppm). The NMR spectra were obtained, and the chemical structures of CO-*g*-DLA and CO-*r*-DLA copolymer were then characterized. For Gel permeation chromatography (GPC), The 1260 Infinity Multi-Detector GPC/SEC System with Refractive Index, Viscometer and dual angle Light Scattering detectors was calibrated using a polystyrene calibrant of 113,000 g/mol. GPC samples were then dissolved in HPLC grade THF at 3 mg/mL as eluent and filtered with a 0.22 µm pore-sized PTFE syringe filter before running on the system with a 5 µm sized column with guard column attachment at flowrate of 1.0 mL min^{-1}. The number (M_n), weight-average molecular weight (M_w), and polydispersity (PDI) of the synthesized fillers were obtained.

Thermal analysis: Thermal stability was evaluated for initial temperature at 5% weight loss (T_{onset}) and decomposition temperature ($T_{d,\ max}$) using TGA (TA Instrument Q500). Approximately 10 mg of sample was placed in an aluminum pan and heated from 30 to 600°C at a step rate of 20°C/min in nitrogen at a flow rate of 60 ml/min.

Additionally, dynamic scanning calorimetry (DSC) (TA Instruments Q100) was used to evaluate the crystallization and melting properties of the fillers, and the resulting biocomposites were characterized using a calorimeter using heat/cool/heat procedure. The employed heating and cooling rate were 10°C/min under a nitrogen flow of 50 ml/min. In this procedure, about 10 mg of the sample was placed in an airtight aluminum pan and heated from 25 to 200 °C to remove any residual thermal history, followed by isothermal for 2 min. Then, samples were cooled to −80 °C, and finally heated (second heating scan) to 200 °C. The thermal transition

temperature such as glass transition (T_g) was taken at the center of heat capacity changes. Contrarily, the melting temperature (T_m) and cold crystallization temperature (T_{cc}) were obtained from the second heating curve. The crystallinity degree (χ_{DSC}) was estimated as shown in equation (i):

$$\chi_{DSC} = \frac{\Delta H_m - \Delta H_{cc}}{\Delta H_m^{\circ} \times w_i} \times 100 \quad \text{(i)}$$

where ΔH_m is the PHB melting enthalpy in the sample, ΔH_m is the cold-crystallization enthalpy, ΔH_m° is the enthalpy of melting for 100% crystalline PHB (ΔH_m°=146 J g^{-1}) and w_i is the weight fraction of filler.

Mechanical Properties: Tensile properties were evaluated using the Instron 5569 Table Universal testing machine following ASTM D638-02. At least five "dumbbell" samples cut from the cast film were stretched at a traverse speed of 5 mm/min (strain rate = 0.5) at room temperature. The resultant tensile modulus, tensile strength, and percent elongation data obtained using Instron Bluehill 3 software were averaged and reported.

Morphological and Structural evaluation: The JEOL JSM 6700F Field Emission Scanning Electron Microscope (FESEM) in transmission mode was used to assess morphological studies on fractured samples and dispersion of fillers within the matrix. On the other hand, Bruker GADDS diffractometer (D8 Discover MR) was employed to capture WAXD patterns for crystal structure insights for PHB and modified PHB composite films. The WAXD diffractograms were obtained as a function of 2θ in the 5-60° range with an area detector operating at 50 kV, 800 μA current, and Cu-K radiation (λ = 1.5418) at room temperature.

SAXS microstructure evolution: The microstructure evolution studies on fractured samples

were done using Small-angle X-ray scattering (Xenocs Xeuss 2.0 SAXS) at 50 kV and 0.6 mA with Cu-Kα radiation (1.5418 Å). The 2D scattering images were reduced to 1D profiles by integration, and intensities in SAXS results were normalized by sample thickness and then Lorentz corrected.

Results and Discussion

Synthesis and molecular characteristics of castor oil-based fillers.

It is well known that catalyzed ROP of cyclic esters such as lactides or lactones using tin(II) octoate initiates at a hydroxyl or amine functional site.[40-42] In this regard, castor oil, which has three secondary hydroxyl groups, was used as an initiator for the polymerization of lactide. ε-caprolactone and D-lactide monomers using stannous octoate in bulk in a solventless system. Nearly all the monomers were consumed during polymerization because the obtained yield was over 90%. **Figure 1a and 1b** shows the synthetic pathways of CO-*g*-DLA (filler a) and CO-*r*-DLA (filler b).

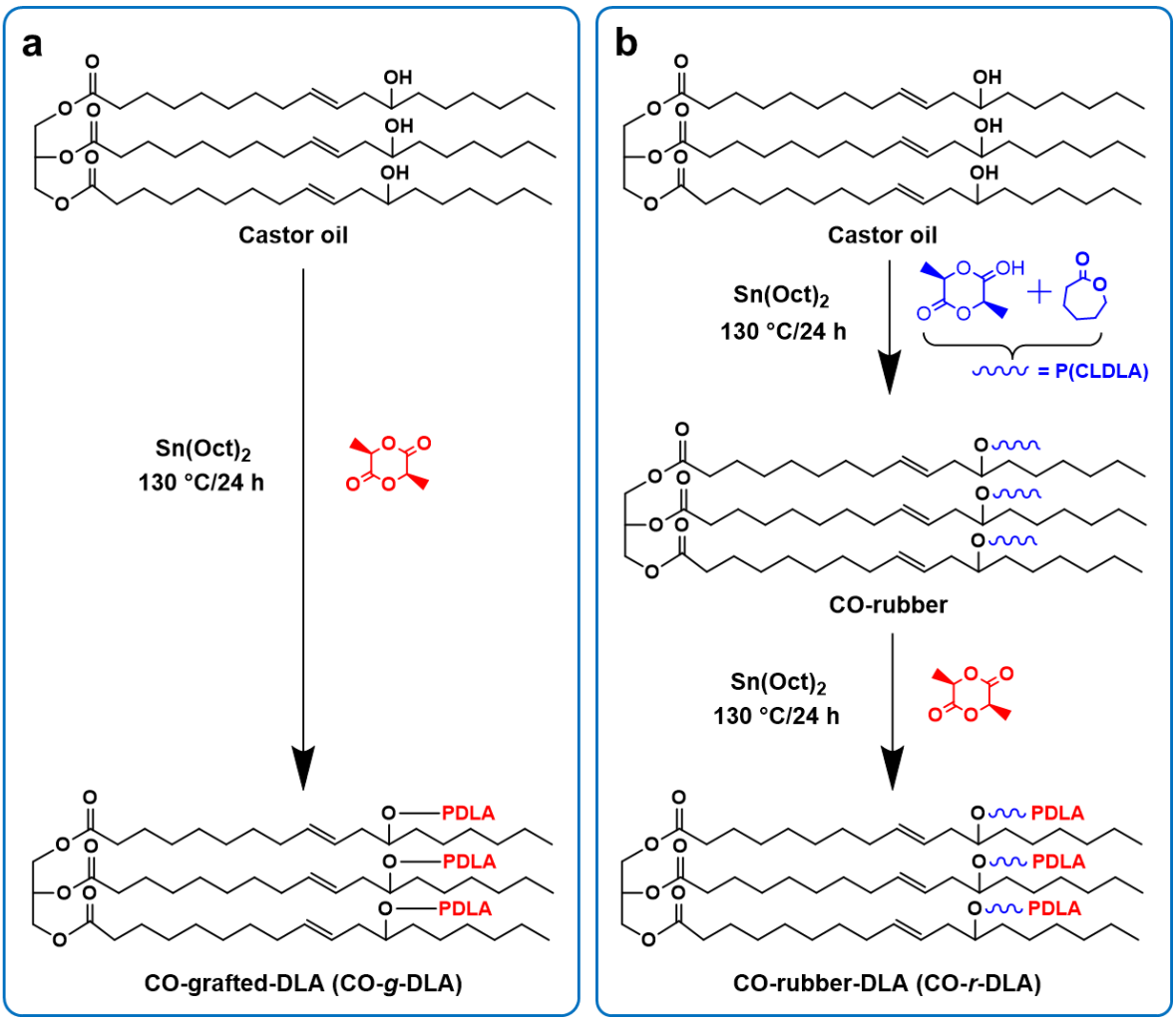

Figure 1. Schematic pathways of the synthesis castor-oil (CO)-based fillers, (a) CO-*g*-DLA and (b) CO-*r*-DLA.

To get insights on the successful grafting of the random sequence P(*CL-co-DLA*) and DLA chain of the filler from the castor-oil surface, molecular structure and molecular weight values were examined using ^{1}H NMR and GPC, respectively, as shown in **Figure 2**. For the ^{1}H NMR, **Figure 2a** shows the assigned protons' local magnetic environment. Then, the resultant peaks of the fillers that confirm the grafting of branched D-lactide and ε-caprolactone are shown in **Figure 2b**. Clearly, in the case of CO-*r*-DLA, there are additional peaks at 4.04 ppm, 2.29 ppm,

1.63 ppm, 1.58 ppm, and 1.24 ppm (labeled as t, p, q, r, and s) compared with CO-*g*-DLA. These resonance peaks are ascribed to the grafted ε-caprolactone. The peaks at 5.15 ppm denote −CH− (labeled as b), while the methyl group has a resonance at 1.5 ppm (labeled as h) for lactide.

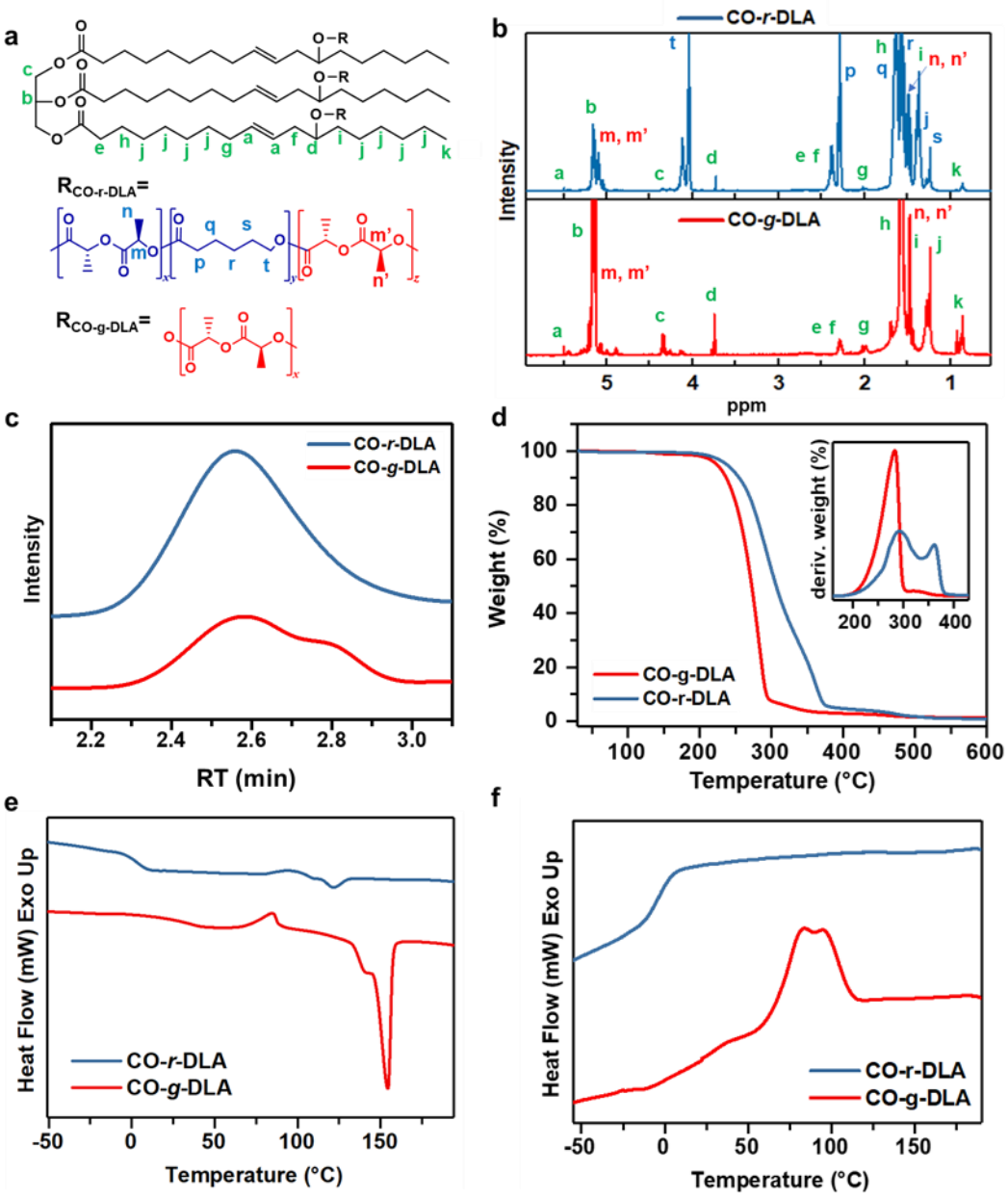

Figure 2. Representations of (a) molecular structures of fillers, (b) ^{1}H NMR spectrum and (c) GPC graph of CO-*r*-DLA and CO-*g*-DLA fillers (d) Thermal stability TGA thermograms and

derivative (DTG) curves (inset), (e) DSC second heating thermograms and (f) cooling thermograms of CO-g-DLA and CO-r-DLA fillers.

The molecular weight (M_w) of a polymer and its distribution, i.e., polydispersity index (PDI), is widely acknowledged as intrinsically related to the polymer's properties. Processability, morphological phase behavior, and thermomechanical performance are some of these qualities that are affected.[43] Therefore, the grafting efficiency related to M_w is determined via molecular weight values obtained by GPC (**Figure 2c).** CO-*g*-DLA depicts a low-intensity and broadened multimodal curve, whereas CO-*r*-DLA is a monomodal broadened GPC graph. The calculated molecular weights M_n and M_w of CO-*g*-DLA and CO-*r*-DLA are 11272 g/mol, 16993 g/mol, and 12756 g/mol, 19496g/mol, respectively, and a PDI (M_w/M_n = ~1.5).

Thermal properties of castor oil-based fillers

More importantly, the thermal parameters of fillers could help identify suitable material for toughening thermoplastics such as PHB. In this regard, TGA analysis is a useful technique to test the thermal stability of materials, whereas DSC provides the thermal behavior of the materials. **Figure 2d** shows the TGA thermograms of CO-*r*-DLA and CO-*g*-DLA fillers with onset thermal decomposition ($T_{95\%}$) located around 255.73 °C and 241.40 °C, respectively. On the other hand, derivative curves (DTGA) in **Figure 2d (inset)** show that CO-*r*-DLA undergoes a 2-step degradation process with maximum degradation peaks ($T_{d,max}$) at 291.9 °C and 359 °C, whereas $T_{d,max}$ of CO-*g*-DLA located at 282.9 °C. These results depict CO-*r*-DLA as more thermally stable compared with CO-*g*-DLA. This higher thermal stability could be ascribed to the two components forming the random copolymer, i.e., caprolactone and a lactide block,

which degrade at different temperatures. In terms of thermal transitions, the CO-g-DLA has a crystallization temperature (T_c) of 83.2 °C during the cooling cycle, a glass transition temperature (T_g) of 36.05 °C and a melting temperature (T_m) of 154.18 °C, as depicted in **Figure 2e and 2f**. On the other hand, incorporating a rubber copolymer in the filler backbone, CO-*r*-DLA, shows a significant difference in the thermal transitions. For instance, there was no T_c observed during the cooling cycle and a sub-temperature T_g was observed at -20.67 °C and 2.45 °C, ascribed to the rubber segment, P(*CL-co-DLA*). Moreover, only a small crystalline phase was observed at a relatively lower T_m at 121.39 °C, after the rubber grafting process.

Having ascertained the critical properties of the fillers, incorporating them into the PHB matrix could produce exciting thermal and mechanical properties for broader applications. For instance, the thermal properties of PHB-filler composites are depicted by TGA/DTG and DSC curves in **Figure 3**. As seen from TG/DTG curves of neat PHB and composite films in **Figure 3 (a, b)** and **Table 1**, adding 20% CO-*r*-DLA and CO-*g*-DLA into PHB reduces the onset decomposition temperature ($T_{95\%}$) of PHB by between 9 – 10 °C, whereas with 10% of the fillers increase the $T_{95\%}$ by about 6 – 9 °C, compared to PHB (shown as inset **Figure 3a,b**). On the other hand, adding 20 % CO-*g*-DLA and 20 % CO-*r*-DLA reduce the $T_{d,max}$ by about 11 °C and 16 °C, respectively, whereas with 10 % copolymer, the $T_{d,max}$ reduce marginally compared to PHB. This decrease in $T_{d,max}$ with adding 20 % copolymer, could be attributed to the filler composition and content. The more flexible random chains comprising ε-caprolactone and D-lactide in CO-*r*-DLA plausibly reduced the thermal stability of the resultant PHB composite film.

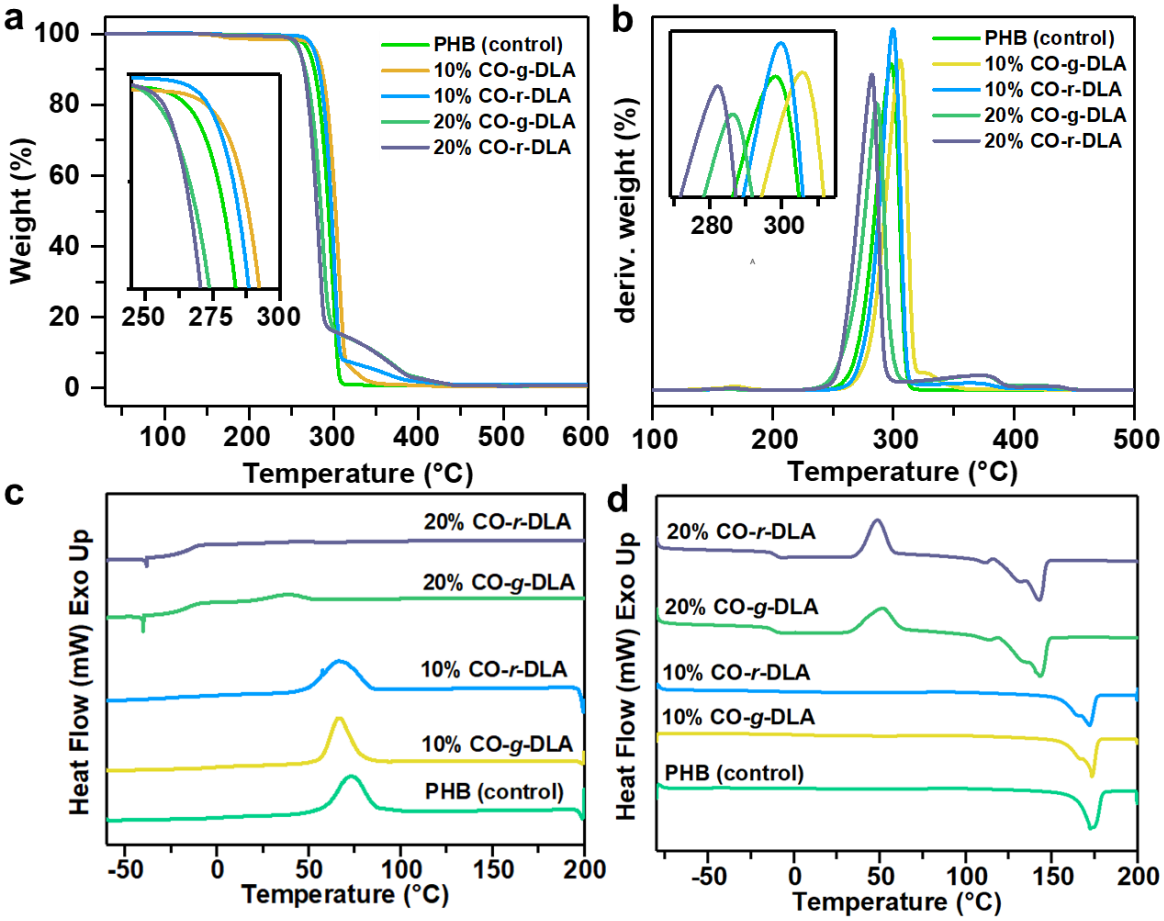

Figure 3. Thermal characteristics (a) TGA curve and (b) derivatives, and (c) DSC heating and (d) cooling thermograms for PHB, PHB/10% CO-*g*-DLA, PHB/10% CO-*r*-DLA PHB/20% CO-*g*-DLA and PHB/20% CO-*r*-DLA.

On the other hand, **Figure 3** (**c,d**) shows DSC second runs depicting the thermal behavior of the resultant composite films. As seen, pure PHB film displays a crystallization temperature (T_c), a glass transition temperature (T_g), a melting temperature (T_m), and crystallinity (χ_c) of 72.94 ℃, 8.35 ℃, 172.41 ℃, 53.2%, respectively. PHB/10% CO-r-DLA and PHB/10% CO-g-DLA show a very close melting temperature and crystallinity compared with PHB. However, increasing the filler content to 20% leads to a dramatic decrease in melting and a noticeable

decrease in T_g. This reduction is attributed to the addition of low T_g filler and castor oil's long aliphatic chain triglycerides, which can diffuse between PHB molecular structure, boosting the free volume and causing a dilution effect.[44, 45]

On the other hand, the PHB composite films exhibit shoulder at the melting stage to form double melting peaks (a minor peak followed by a significant peak at higher temperatures). This result could be ascribed to either the presence of the two crystal distinct forms (α and β crystals) or melting, re-crystallization, and re-melting process.[46, 47] Crystallinity refers to the degree of molecular order within a polymer chain, where higher crystallinity implies a more ordered structure. Notably, neat PHB had a crystallinity of 53.2%, which agrees with that reported in the literature.[48] The crystallinity slightly increased or decreased by including the synthesized fillers in varied content. For instance, adding 10% CO-*r*-PDLA increased the crystallinity to about 55.3%, whereas the PHB composite with 20% CO-*g*-PDLA resulted in a lower crystallinity of 47.3%, as shown in **Table 1.** The varied crystallinity values would likely affect the overall mechanical properties of the PHB/filler films. This is because higher crystallinity enhances stiffness and strength in polymers, but may make them brittle due to stress concentration, while lower crystallinity improves toughness by promoting molecular mobility and energy dissipation.[49, 50] The overall thermal properties of the fillers and the resultant PHB composite films are summarized in **Table 1**.

Table 1. Thermal properties of castor oil-based fillers (CO-*g*-DLA and CO-*r*-DLA), PHB and its green biocomposite films

Samples	TGA		DSC					
	$T_{95\%}$ (˚C)	$T_{d,max}$ (˚C)	T_c (˚C)	ΔH_c (J/g)	T_g (˚C)	T_m (˚C)	ΔH_m (J/g)	χ_c (%)
Fillers								
CO-*g*-DLA	223.8	282.4	83.2	28.2	36.05	154.18	44.88	-
CO-*r*-DLA	237.2	293.3/363.5	-	-	-20.67, 2.45	121.39	3.6	-
Composite films								
PHB	270.8	298.4	72.94	58.13	8.35	172.41	77.74	53.2
10% CO-*g*-DLA	279.2	305.7	66.27	49.96	-0.77	173.3	71.53	54.4
20% CO-g-DLA	259.8	287.1	51.71	40.76	-12.36	133.68/142.52	55.25	47.3
10% CO-*r*-DLA	277.3	299.9	66.13	51.20	-21.96	171.94	72.7	55.3
20% CO-*r*-DLA	260.5	282.1	48.70	47.99	-10.88	131.02/142.75	61.34	52.5

$T_{95\%}$ = initial degradation temperature, $T_{d,max}$ = max decomposition temperature, T_c = Crystallization temperature, ΔH_c = Enthalpy of crystallization, T_g = glass transition temperature, T_m = melting temperature, ΔH_c = Enthalpy of melting, χ_c = crystallinity

Mechanical performance of PHB green biocomposites

The macroscopic behavior of a composite is an important parameter to consider and is usually depicted by a stress-strain curve.[51] In this regard, the mechanical properties of neat PHB were examined in relation to that of modified PHB with CO-*g*-DLA and CO-*r*-DLA fillers, as shown in **Figure 4a**

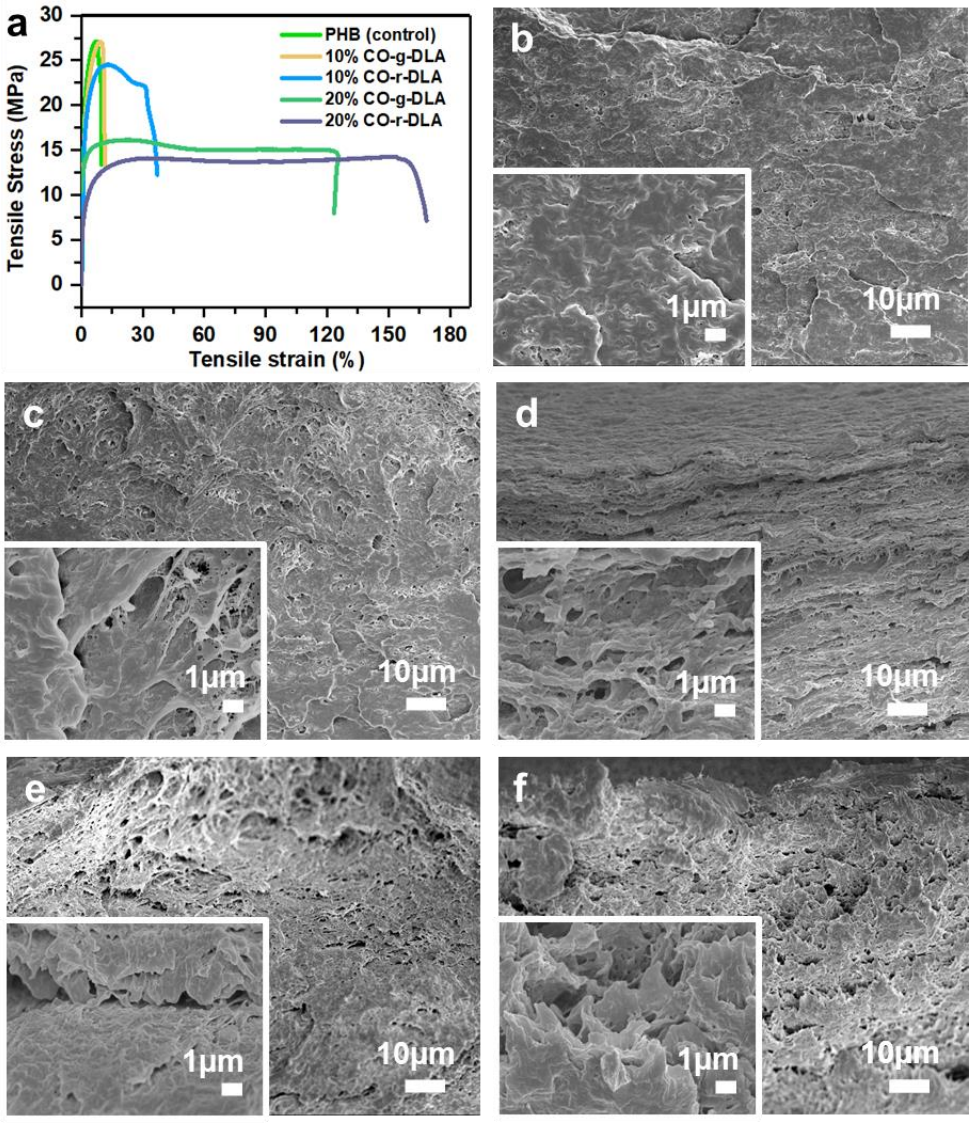

Figure 4. (a) Tensile properties graph of PHB, PHB/10% CO-g-DLA, PHB/20% CO-r-DLA and PHB/20% CO-g-DLA and PHB/20% CO-r-DLA. FESEM cross-sectional images of tensile fractured surfaces (b) PHB, (c) PHB/10% CO-g-DLA, (d) PHB/10% CO-r-DLA, (e) PHB/20%

CO-g-DLA and (f) PHB/20% CO-r-DLA.

As the stress-strain curves show, PHB film is typically a brittle polymer with Young's modulus, tensile strength, and elongation at break of about 1.71 GPa, 24.73 MPa, and 10.34%, respectively. The low elongation at break with no plastic deformation in PHB limits its widespread application where flexibility is a critical requirement, such as in sustainable packaging.[52] However, the PHB polymer properties can be significantly altered by designing and incorporating low T_g or rigid fillers. Intriguingly, from **Figure 4a**, adding 10% CO-*r*-PDLA enhanced the elongation at break by 3-fold, whereas 10% CO-*g*-PDLA did not significantly improve the flexibility (ε =12.21%) of the resultant PHB composite compared to neat PHB. However, the strength and Young's modulus remain almost identical. On the other hand, composites with 20% CO-*r*-PDLA and 20% CO-*g*-PDLA resulted in about 13-fold improvement in elongation at break, but with about 50% and 16-18% reduction strength and Young's modulus, respectively, compared with neat PHB. Although CO-*g*-PDLA filler could be considered rigid, the high content (20%) produces comparable mechanical properties with PHB/20% CO-*r*-PDLA composite. With high filler content, the resulting PHB composite films show exceptional tensile toughness compared with that of neat PHB and low filler content films, as summarized in **Table 2**.

Table 2. Mechanical characteristics of PHB and its biocomposite films

Samples	**Mechanical Properties**			
	E (GPa)	**σ (MPa)**	**ε (%)**	**Toughness ($MJ \cdot m^{-3}$)**
PHB	1.71 ± 0.12	24.73 ± 3.17	10.34 ± 2.72	2.82 ± 0.98
10% CO-*g*-DLA	1.82 ± 0.14	26.68 ± 0.61	12.21 ± 2.49	3.02 ± 0.40
20% CO-*g*-DLA	1.43 ± 0.40	12.22 ± 1.64	127.49 ± 3.39	18.24 ± 0.85
10% CO-*r*-DLA	1.75 ± 0.20	24.57 ± 1.71	29.68 ± 8.34	6.34 ± 1.36

20% CO-*r*-DLA	1.39 ± 0.21	12.05 ± 2.80	143.15 ± 15.19	19.01± 1.33

Notably, the 20% loadings of both CO-*r*-DLA and CO-*g*-DLA offer similar toughening effects in PHB due to a sufficient volume of fillers to enhance the overall composite film properties.[53] However, the differentiation arises when the filler is introduced at a lower concentration (10%), likely indicating that the CO-*r*-DLA possesses superior compatibility with the PHB matrix, resulting in more effective stress transfer and toughening mechanisms, whereas the 10% CO-*g*-DLA filler may not exhibit the same level of compatibility and mechanical synergy, leading to less substantial toughening in the PHB matrix.[54] Based on the resultant optimal mechanical properties for PHB composite films with 20% filler (E=1.4 GPa, σ=12 MPa, ε =130%), the film has potential to replace polyethylene (PE) which has comparable properties depending on the grades such as high-density polyethylene (HDPE).[55]These PHB composite films could find applications in housewares, toys and food containers to replace the HDPE 25055E grade. It is worth noting that although these results are promising, further research is necessary to determine the suitability of the PHB composite as a substitute for HDPE plastic in terms of cost, availability, and other performance requirements such as barrier properties.[56] PHB has been reported to have moderate to good barrier properties to shield the foodstuff from light, air, water vapor, and smell components, which eventually prevents its deterioration. However, modifying PHB using various fillers to achieve specific mechanical properties (flexibility, toughness) may also involve a trade-off with other properties such as barrier performance.[57] Compared with the pore-free approaches, the considerably enhanced mechanical properties of PHB by plant oil fillers presented in this study could also lead to formation of pores that

increase the permeation and diffusion, altering the innate barrier properties of the modified PHB as packaging materials. This is in good agreement with previous report on using plasticizer for the mechanical properties improvement as packaging materials.[58]

On the other hand, PHB composite film offers several benefits in addressing environmental pollution issues compared to traditional plastic packaging. For instance, it can undergo biodegradation, breaking down into natural compounds over time, reducing plastic waste accumulation in landfills and water bodies.[3, 59] Moreover, biodegradation enriches soil health and ecosystem functioning, promoting microbial activity and promoting sustainable agricultural practices.[60] In addition, proper disposal also reduces microplastic generation, safeguarding marine ecosystems and human well-being. Furthermore, the PHB-based films with a biopolymer produced by microbial fermentation of renewable carbon sources, reduces reliance on fossil fuels and minimizes the carbon footprint. More importantly, these biodegradable packaging materials align with the principles of a circular economy, for instance, by converting PHB composite films into valuable organic matter or biogas for energy generation.[4, 9, 60]

Morphological analysis of PHB green biocomposites

Understanding material performance and durability by comparing mechanical properties to morphological characteristics of broken samples is crucial for comprehending failure mechanisms and creating more resilient composites.[61] In this respect, the morphological features of the tensile fractured films were studied FESEM. **Figure 4 (b-f)** shows the resulting FESEM morphological features of a tensile bar cross-section of PHB and selected PHB

composite films. As seen in **Figure 4b**, PHB film exhibits a brittle fracture failure with insignificant yielding after the elastic deformation. This observation agrees with the elongation at break of about 10% obtained in the tensile data and perfectly agrees with previous studies.[62] On the other hand, the PHB composite films incorporating 10% CO-*g*-DLA filler show a brittle failure in **Figure 4c** and a ductile failure with 10% CO-*g*-DLA in **Figure 4d**. As found in other studies, the ductile failure mode for PHB/10% CO-r-DLA is characterized by rough fracture surfaces ascribed to resistance to break or deformation.[63] Concerning PHB/10% CO-*g*-DLA samples, the filler induces some plastic deformation, resulting in a coarser surface, probably due to hydrogen bond interactions between the PHB and PDLA blocks in the filler. In agreement, the results have shown that star-branched block fillers in PLA matrix display similar features.[64, 65] Notably, with increased content of fillers up to 20% CO-*g*-DLA and CO-*r*-DLA, as seen in **Figure 4e** and **4f**, the fractured surfaces of the composite films appear rougher, an indication of not only enhanced tearing resistance but also high deformation as evidenced by the strain at break of about 130%.[66] Besides morphological features, structural properties of composite materials are crucial in achieving the desired balance of mechanical strength, durability, and performance, which determines the material's behavior and suitability for specific applications.[11]

Crystal structure of PHB green biocomposites

A particularly useful tool for tracking the structural evolution of semi-crystalline polymers is WAXD-SAXS analysis[11] as seen in **Figure 5**. The wide-angle X-ray diffraction (WAXD) shown in **Figure 5a** reveals the crystal structure of PHB and the selected composite films.

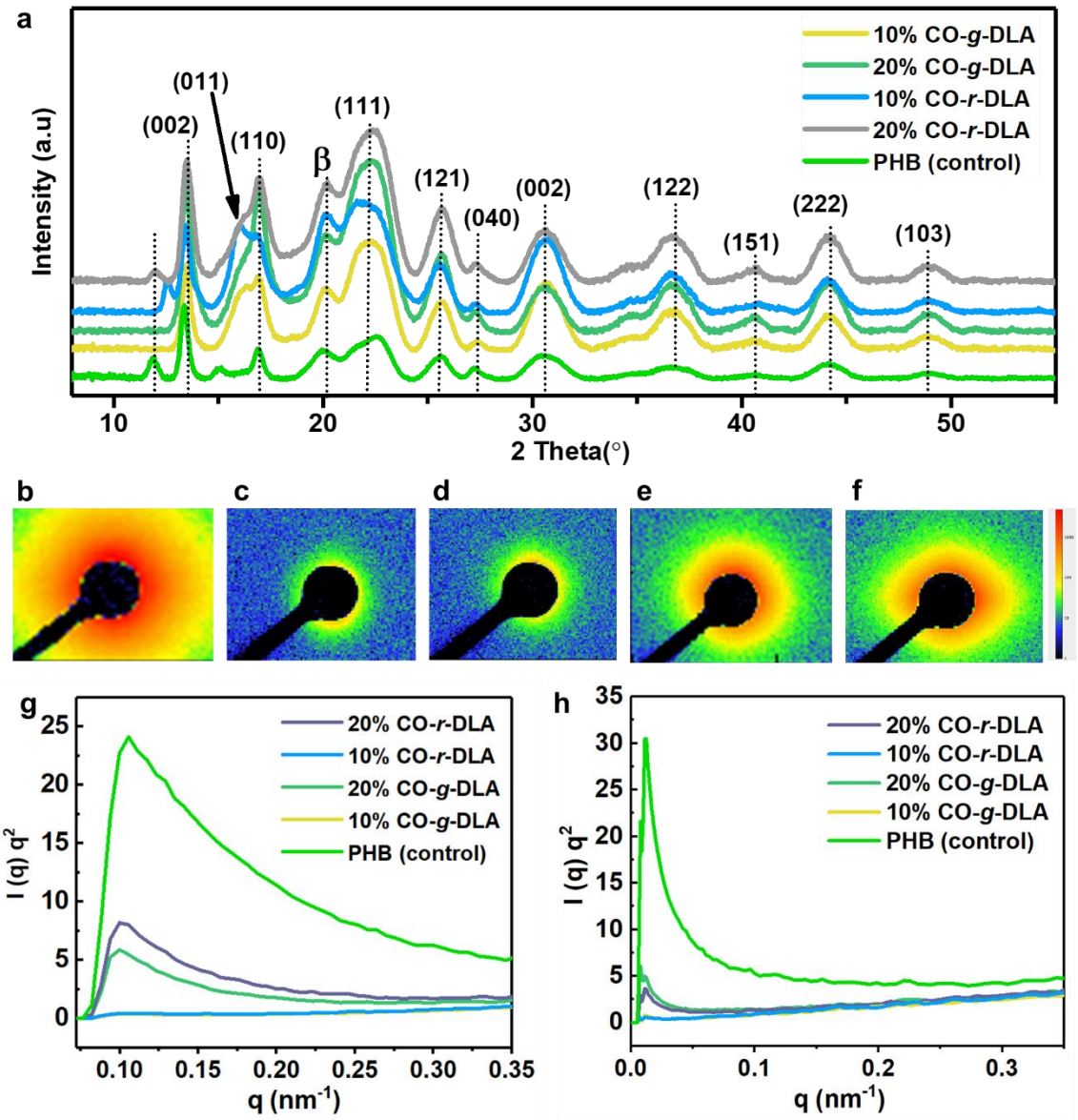

Figure 5. Structural evolution of PHB and selected composite films (a) WAXD intensity profiles for the PHB and its composite films. 2D SAXS patterns of selected samples (b) PHB, (c) PHB/10% CO-*g*-DLA, (d) PHB/10% CO-*r*-DLA, (e) PHB/20% CO-*g*-DLA, and (f) PHB/20% CO-*r*-DLA, and Lorentz corrected 1-D SAXS profiles in the (g) equatorial direction and (h) meridional direction.

As seen in the WAXD structure analysis, PHB crystallizes in an orthorhombic crystal structure with its prominent peaks displayed at 2θ angles of 13.95°, 16.84°, 20.5°, 22.7°, 25.9°, 27.7°,

30.9° and 36.7°, associated with crystallographic planes (020), (110), (111), (121), (040), (002) and (122), respectively.[67] Other peaks are observed at 2θ values of 40.7°, 44.2°, and 49° representing the (151), (222), and (103) indices. Interestingly, all the modified PHB composite films depict similar peaks with neat PHB, and the expected additional peaks for PDLA and PCL blocks (i.e., 16.5°, 21°, 22.5°, and 34.5°) seem to be overlapped by those of neat PHB. This dominance notwithstanding, these results clearly show that the structural data of the neat PHB is not significantly altered by the inclusion of the synthesized fillers except for the slight increase or decrease in crystallinity as observed in the DSC data.[49, 68, 69] To collaborate the double melting DSC profiles, PHB and resulting composites show the presence of a peak at around 2θ = 20° attributed to β form crystals[70], which confirms that the melting peaks result from the presence of two crystal distinct forms.

Microstructural evolution and toughening mechanism of PHB green biocomposite

From literature, PHB forms large ring band spherulites during crystallization, eventually leading to cracks or unstable multiple crazing deformations during brittle failure.[71] On the other hand, modification of PHB with castor-oil fillers could interfere with the ring banding, help form smaller spherulites, and reduce crystallinity. Such modifications could alter the PHB's deformation behavior and induce toughening via mechanisms such as mixed crazing or shear yielding or both.

It is worth noting that the toughening mechanisms result from microstructure change, which eventually dictate the failure modes as well as the resultant mechanical performance of the PHB composite films compared with that of neat PHB. For instance, incorporation of 20 %

filler recorded about 13-fold enhancement in flexibility (ductility) compared with the brittle PHB film. Importantly, CO-*r*-DLA filler comprises a flexible phase that could alter the deformation of the PHB matrix by a shear-yielding and fibrillation mechanism. As expected, the resultant fracture morphology shows irregular and uneven features with fibrils along the surface, as depicted in **Figure 4.** Interestingly**,** CO-*g*-DLA though regarded as a rigid polymer, also result in highly ductile PHB film contrary to the expectation, plausibly because of enhanced interactions between PHB and the high filler content.

It is imperative to study the microstructure evolution to get insights on tensile deformation mechanism and correlation between structure and performance of materials. During tensile deformation, Small-angle X-ray scattering (SAXS) is a useful technique to study the tensile deformation mechanism of semi-crystalline polymers such as PHB.[72] The microstructure evolution in PHB and the resulting film in our study is of tremendous interest because of the potential of castor oil-based fillers to act craze initiators and thus determine the resultant mechanical performance. SAXS can help trace inhomogeneities, domain separation, crazes, or lamellar stacks in PHB and composite films.[11] For example, SAXS is renowned for tracing craze formation (~10-1000Å) in polymer matrices by detecting 2D scattering of craze fibrils at small angles ($< 2\theta = 10°$).[24] Craze formation in meridional and equatorial directions typically produces a cross-like SAXS signature. **Figure 5 (b-h)** shows the microstructure evolution in neat PHB and selected PHB composite films with 10% and 20% CO-*g*-PDLA and CO-*r*-PDLA fillers. **Figure 5 (b-f)** shows that selected samples produce different 2D SAXS profiles depending on the resultant microstructure. To interpret the structural information in the 2D SAXS profiles, radial integration was used to reduce the 2D scattering data into 1D plots of

scattering intensity (y-axis) versus q-value (x-axis). The 1D plots are Lorentz corrected to obtain scattering invariant Q calculated from equation (ii):

$$Q = \int I(q) q^2 \, dq \qquad \text{(ii)}$$

where Q is the scattering invariant, and q is the scattering vector which equals $4\pi \sin(\theta)/\lambda$ (nm^{-1}).[73] Notably, the Lorentz correction shifts a broad correlation peak to higher values of q by multiplying the intensity function by a factor of q^2.[48]

From the 2D profiles, although all the selected samples show isotropic rings, PHB diffraction rings are more pronounced than the composites. These results could be attributed to the formation of crazes in PHB, which creates microscopic voids visible as whitening when stretched.[48] These strong crazes form in the equatorial direction and meridional crack planes, resulting in a near-circular 2D scattering pattern and high-intensity 1D profile, as shown in **Figure 5b** and **Figure 5 (g, h)**, respectively. As a result, as the PHB polymer is stretched more, the fibrils lengthen until they fail and form a crack. Contrarily, PHB composite films contain inhomogeneities that act as stress concentrators because of differences in elastic properties in relation to the PHB matrix but also help to absorb large amounts of energy before failure as it elongates. As seen in **Figure 5 (c, d)**, with 10% filler content, the scattering intensities are much lower than in PHB. These results attest to the fact that the fillers not only disrupt the formation of cracks but also the deformation mechanism. In the case of PHB/10% CO-*r*-DLA, there is more extensive deformation before break compared with that of PHB/10% CO-*g*-DLA, probably because of the matrix's strong interactions and the former's softer phase. However, the scattering intensities from both fillers are nearly similar in both directions, as shown in **Figure 5 (g, h)**. However, by increasing the filler contents to 20%, the 2D scattering pattern

and 1D intensities are enhanced for both fillers in the equatorial direction and meridional crack planes during deformation, as seen in **Figure 5 (e, f)** and **Figure 5 (g, h)**, respectively. The results reveal that filler content could increase matrix interactions and delay the failure during deformation. Based on the experimental findings, **Figure 6** presents a schematic representation of the proposed toughening mechanism of PHB composite films. As seen, when PHB polymer is stretched above the yield point, the fibrils lengthen until they fail and form a crack.

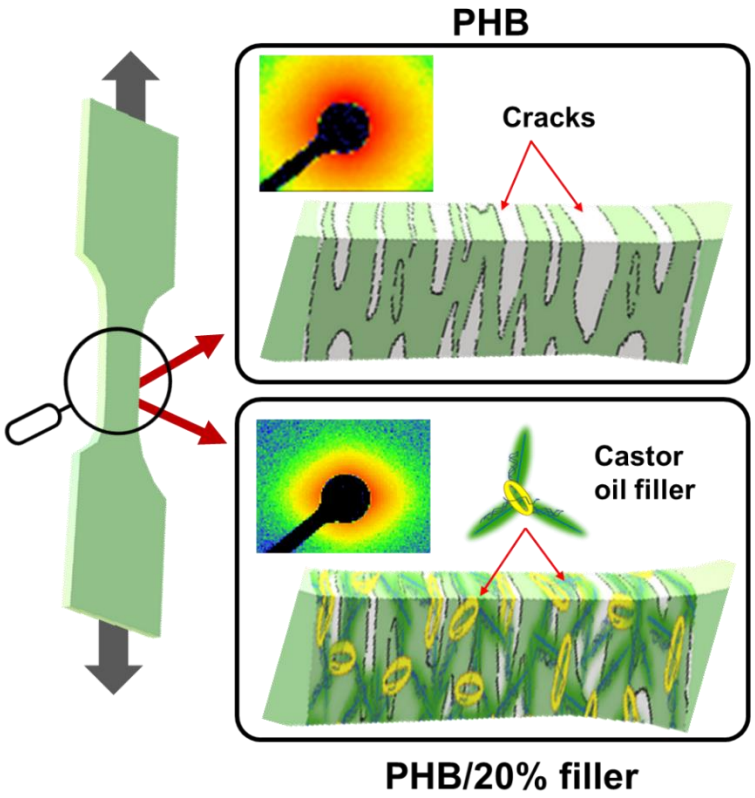

Figure 6. Schematic representation of the toughening mechanism of PHB and PHB/20% filler composite film during uniaxial stretching.

On the other hand, inclusion of castor-oil fillers (~ 20%) result in excessive deformation from localized shear yielding and fibrillation as depicted by FESEM features in **Figure 4f**. This deformation behavior could be attributed to the substantial interfacial interactions between the

matrix and the much softer fillers as well as plasticizing effect of castor-oil backbone. The proposed mechanism is also in agreement with the mechanical properties data in **Table 2**, showing that 20% CO-*r*-DLA and 20% CO-*g*-DLA filler resulted in about 13-fold improvement in elongation at break, whereas 10% CO-*r*-DLA filler was only effective by about 3-fold. Additionally, the effect induced by crystallinity of PHB/filler composite films as shown in **Table 1**, cannot be underestimated. As seen, lower crystallinity enhances polymer toughness by promoting molecular mobility and energy dissipation mechanisms and allow films to absorb more energy before failure.[49] These results underscore the importance of filler content, filler structure, and matrix-filler interactions in optimizing the mechanical properties of composite materials.

Conclusion

In summary, this study presents a breakthrough in the synthesis of sustainable materials for packaging applications. We studied the green synthesis of castor oil-based filler for Poly(3-hydroxybutyrate) (PHB) toughening and showed that addition of these filler (20%) effectively mitigated PHB's brittleness by promoting fibrillation, ultimately enhancing its toughness. Moreover, the importance of filler content and structure, and matrix-filler interactions in optimizing the mechanical properties of composite materials is elucidated. The potential application of biodegradable PHB composite films as alternative to conventional plastics, especially some HDPE grades, is significant in the sustainable packaging field. Overall, this study is important in terms of sustainability as it provides valuable insights into the use of sustainable and environmentally friendly fillers for enhancing the properties of biodegradable

polymers. The development of sustainable and biodegradable materials is an important step towards addressing the challenges of plastic pollution and promoting a more sustainable future.

Conflicts of interest

The authors declare that they have no known competing financial interests.

Acknowledgements

This project is supported by RIE2025 Manufacturing, Trade and Connectivity (MTC) Programmatic Fund (M22K9b0049), AME Young Individual Research Grants (YIRG) (Grant No. A2084c0168) and GAP Grant (Grant No. I22D1AG014) administrated by A*STAR.

References

1. MacLeod, M.; Arp, H. P. H.; Tekman, M. B.; Jahnke, A., The global threat from plastic pollution. *Science* **2021,** *373* (6550), 61-65.

2. Bergmann, M.; Almroth, B. C.; Brander, S. M.; Dey, T.; Green, D. S.; Gundogdu, S.; Krieger, A.; Wagner, M.; Walker, T. R., A global plastic treaty must cap production. *Science* **2022,** *376* (6592), 469-470.

3. Rosenboom, J.-G.; Langer, R.; Traverso, G., Bioplastics for a circular economy. *Nature Reviews Materials* **2022,** *7* (2), 117-137. 10.1038/s41578-021-00407-8.

4. Mohanty, A. K.; Wu, F.; Mincheva, R.; Hakkarainen, M.; Raquez, J.-M.; Mielewski, D. F.; Narayan, R.; Netravali, A. N.; Misra, M., Sustainable polymers. *Nature Reviews Methods Primers* **2022,** *2* (1), 46. 10.1038/s43586-022-00124-8.

5. Li, Z.; Muiruri, J. K.; Thitsartarn, W.; Zhang, X.; Tan, B. H.; He, C., Biodegradable silica rubber core-shell nanoparticles and their stereocomplex for efficient PLA toughening. *Composites Science and Technology* **2018,** *159*, 11-17.

6. Wendels, S.; Heinrich, B.; Donnio, B.; Avérous, L., Green and controlled synthesis of short diol oligomers from polyhydroxyalkanoate to develop fully biobased thermoplastics. *European Polymer Journal* **2021,** *153*, 110531.

7. McChalicher, C. W.; Srienc, F., Investigating the structure–property relationship of bacterial PHA block copolymers. *Journal of biotechnology* **2007,** *132* (3), 296-302.

8. Westlie, A. H.; Quinn, E. C.; Parker, C. R.; Chen, E. Y. X., Synthetic biodegradable polyhydroxyalkanoates (PHAs): Recent advances and future challenges. *Progress in Polymer Science* **2022,** *134*, 101608. https://doi.org/10.1016/j.progpolymsci.2022.101608.

9. Zhou, L.; Zhang, Z.; Shi, C.; Scoti, M.; Barange, D. K.; Gowda, R. R.; Chen, E. Y.-X., Chemically circular, mechanically tough, and melt-processable polyhydroxyalkanoates. *Science* **2023,** *380* (6640), 64-69. doi:10.1126/science.adg4520.

10. Muiruri, J. K.; Yeo, J. C. C.; Soo, X. Y. D.; Wang, S.; Liu, H.; Kong, J.; Cao, J.; Tan, B. H.; Suwardi, A.; Li, Z., Recent Advances of Sustainable Short-chain length Polyhydroxyalkanoates (Scl-PHAs)–Plant Biomass Composites. *European Polymer Journal* **2023**, 111882.

11. Yeo, J. C. C.; Muiruri, J. K.; Tan, B. H.; Thitsartarn, W.; Kong, J.; Zhang, X.; Li, Z.; He, C., Biodegradable PHB-rubber copolymer toughened PLA green composites with ultrahigh extensibility. *ACS Sustainable Chemistry & Engineering* **2018,** *6* (11), 15517-15527.

12. Huang, W.; Shi, Y.; Wang, W.; Sheng, Y.; Guo, Y.; Li, Y.; Yang, Q.; Chen, P., Polylactide/poly[(R)-3-hydroxybutyrate] (PHB) blend fibers with superior heat-resistance: Effect of PHB on crystallization. *Polymers for Advanced Technologies* **2023,** *34* (5), 1479-1491. https://doi.org/10.1002/pat.5982.

13. Sinisi, A.; Degli Esposti, M.; Braccini, S.; Chiellini, F.; Guzman-Puyol, S.; Heredia-Guerrero, J. A.; Morselli, D.; Fabbri, P., Levulinic acid-based bioplasticizers: a facile approach to enhance the thermal and mechanical properties of polyhydroxyalkanoates. *Materials Advances* **2021,** *2* (24), 7869-7880. 10.1039/D1MA00833A.

14. Mangeon, C.; Michely, L.; Rios de Anda, A.; Thevenieau, F.; Renard, E.; Langlois, V., Natural Terpenes Used as Plasticizers for Poly(3-hydroxybutyrate). *ACS Sustainable Chemistry & Engineering* **2018,** *6* (12), 16160-16168. 10.1021/acssuschemeng.8b02896.

15. Ollier, R. P.; D'Amico, D. A.; Schroeder, W. F.; Cyras, V. P.; Alvarez, V. A., Effect of clay treatment on the thermal degradation of PHB based nanocomposites. *Applied Clay Science* **2018,** *163*, 146-152. https://doi.org/10.1016/j.clay.2018.07.025.

16. Popa, M. S.; Frone, A. N.; Radu, I. C.; Stanescu, P. O.; Truşcă, R.; Rădiţoiu, V.; Nicolae, C. A.; Gabor, A. R.; Panaitescu, D. M., Microfibrillated Cellulose Grafted with Metacrylic Acid as a Modifier in Poly (3-hydroxybutyrate). *Polymers* **2021,** *13* (22), 3970.

17. Dong, W.; Ma, P.; Wang, S.; Chen, M.; Cai, X.; Zhang, Y., Effect of partial crosslinking on morphology and properties of the poly(β-hydroxybutyrate)/poly(d,l-lactic acid) blends. *Polymer Degradation and Stability* **2013,** *98* (9), 1549-1555. https://doi.org/10.1016/j.polymdegradstab.2013.06.033.

18. Briassoulis, D.; Tserotas, P.; Athanasoulia, I.-G., Alternative optimization routes for improving the performance of poly(3-hydroxybutyrate) (PHB) based plastics. *Journal of Cleaner Production* **2021,** *318*, 128555. https://doi.org/10.1016/j.jclepro.2021.128555.

19. Li, Z.; Yang, J.; Loh, X. J., Polyhydroxyalkanoates: opening doors for a sustainable future. *NPG Asia Materials* **2016,** *8* (4), e265-e265. 10.1038/am.2016.48.

20. Pryadko, A.; Surmeneva, M. A.; Surmenev, R. A., Review of hybrid materials based on polyhydroxyalkanoates for tissue engineering applications. *Polymers* **2021,** *13* (11), 1738.

21. Muthuraj, R.; Valerio, O.; Mekonnen, T. H., Recent developments in short- and medium-chain- length Polyhydroxyalkanoates: Production, properties, and applications. *International Journal of Biological Macromolecules* **2021,** *187*, 422-440. https://doi.org/10.1016/j.ijbiomac.2021.07.143.

22. Yeo, J. C. C.; Ong, X. Y.; Koh, J. J.; Kong, J.; Zhang, X.; Thitsartarn, W.; Li, Z.; He, C., Dual-Phase Poly(lactic acid)/Poly(hydroxybutyrate)-Rubber Copolymer as High-Performance Shape Memory Materials. *ACS Applied Polymer Materials* **2021,** *3* (1), 389-399. 10.1021/acsapm.0c01158.

23. Yeo, J. C. C.; Kai, D.; Teng, C. P.; Lin, E. M. J. R.; Tan, B. H.; Li, Z.; He, C., Highly washable and reusable green nanofibrous sorbent with superoleophilicity, biodegradability, and mechanical robustness. *ACS Applied Polymer Materials* **2020,** *2* (11), 4825-4835.

24. Yeo, J. C. C.; Muiruri, J. K.; Koh, J. J.; Thitsartarn, W.; Zhang, X.; Kong, J.; Lin, T. T.; Li, Z.; He, C., Bend, twist, and turn: First bendable and malleable toughened PLA green composites. *Advanced Functional Materials* **2020,** *30* (30), 2001565.

25. Chaos, A.; Sangroniz, A.; Gonzalez, A.; Iriarte, M.; Sarasua, J.-R.; del Río, J.; Etxeberria, A., Tributyl citrate as an effective plasticizer for biodegradable polymers: effect of plasticizer on free volume and transport and mechanical properties. *Polymer International* **2019,** *68* (1), 125-133. https://doi.org/10.1002/pi.5705.

26. Carvalho, N. K.; Silva, A. P. B.; Lemes, A. P., Effects of tributyrin as plasticizer in poly(3-hydroxybutyrate-co-3-hydroxyvalerate) on processability, mechanical, and thermal properties. *Journal of Applied Polymer Science* **2023,** *140* (32), e54249. https://doi.org/10.1002/app.54249.

27. Briassoulis, D.; Athanasoulia, I.-G.; Tserotas, P., PHB/PLA plasticized by olive oil and carvacrol solvent-cast films with optimised ductility and physical ageing stability. *Polymer Degradation and Stability* **2022,** *200*, 109958. https://doi.org/10.1016/j.polymdegradstab.2022.109958.

28. Panaitescu, D. M.; Nicolae, C. A.; Gabor, A. R.; Trusca, R., Thermal and mechanical properties of poly (3-hydroxybutyrate) reinforced with cellulose fibers from wood waste. *Industrial crops and products* **2020,** *145*, 112071.

29. Kumari, S. V. G.; Pakshirajan, K.; Pugazhenthi, G., Facile fabrication and characterization of novel antimicrobial and antioxidant poly (3-hydroxybutyrate)/essential oil composites for potential use in active food packaging applications. *International Journal of Biological Macromolecules* **2023**, 126566.

30. Williams, C. K.; Gregory, G. L., High-performance plastic made from renewable oils is chemically recyclable by design. Nature Publishing Group UK London: 2021.

31. Mutlu, H.; Meier, M. A., Castor oil as a renewable resource for the chemical industry. *European Journal of Lipid Science and Technology* **2010,** *112* (1), 10-30.

32. Hosoda, N.; Lee, E.-H.; Tsujimoto, T.; Uyama, H., Phase Separation-Induced

Crystallization of Poly(3-hydroxybutyrate-co-hydroxyvalerate) by Branched Poly(lactic acid). *Industrial & Engineering Chemistry Research* **2013,** *52* (4), 1548-1553. 10.1021/ie3011275.

33. Yeganeh, H.; Hojati-Talemi, P., Preparation and properties of novel biodegradable polyurethane networks based on castor oil and poly (ethylene glycol). *Polymer degradation and stability* **2007,** *92* (3), 480-489.

34. Karak, N.; Rana, S.; Cho, J. W., Synthesis and characterization of castor-oil-modified hyperbranched polyurethanes. *Journal of Applied Polymer Science* **2009,** *112* (2), 736-743.

35. Dicks, J. A.; Woolard, C., Biodegradable Polymeric Foams Based on Modified Castor Oil, Styrene, and Isobornyl Methacrylate. *Polymers* **2021,** *13* (11), 1872.

36. Ebata, H.; Toshima, K.; Matsumura, S., Lipase-catalyzed synthesis and curing of high-molecular-weight polyricinoleate. *Macromolecular bioscience* **2007,** *7* (6), 798-803.

37. Slivniak, R.; Domb, A. J., Lactic acid and ricinoleic acid based copolyesters. *Macromolecules* **2005,** *38* (13), 5545-5553.

38. Arrieta, M. P.; Perdiguero, M.; Fiori, S.; Kenny, J. M.; Peponi, L., Biodegradable electrospun PLA-PHB fibers plasticized with oligomeric lactic acid. *Polymer Degradation and Stability* **2020,** *179*, 109226.

39. Sokolsky-Papkov, M.; Domb, A. J., Stereoisomeric effect on in vitro drug release from injectable poly (lactic acid co castor oil) polyesters. *Polymers for Advanced Technologies* **2008,** *19* (6), 671-679.

40. Pitet, L. M.; Hait, S. B.; Lanyk, T. J.; Knauss, D. M., Linear and branched architectures from the polymerization of lactide with glycidol. *Macromolecules* **2007,** *40* (7), 2327-2334.

41. Gottschalk, C.; Frey, H., Hyperbranched polylactide copolymers. *Macromolecules* **2006,** *39* (5), 1719-1723.

42. Alba, A.; du Boullay, O. T.; Martin-Vaca, B.; Bourissou, D., Direct ring-opening of lactide with amines: application to the organo-catalyzed preparation of amide end-capped PLA and to the removal of residual lactide from PLA samples. *Polymer Chemistry* **2015,** *6* (6), 989-997. 10.1039/C4PY00973H.

43. Walsh, D. J.; Schinski, D. A.; Schneider, R. A.; Guironnet, D., General route to design polymer molecular weight distributions through flow chemistry. *Nature Communications* **2020,** *11* (1), 3094. 10.1038/s41467-020-16874-6.

44. Xuan, W.; Odelius, K.; Hakkarainen, M., Tailoring oligomeric plasticizers for polylactide through structural control. *Acs Omega* **2022,** *7* (16), 14305-14316.

45. Darie-Niță, R. N.; Irimia, A.; Grigoraș, V. C.; Mustață, F.; Tudorachi, N.; Râpă, M.; Ludwiczak, J.; Iwanczuk, A., Evaluation of Natural and Modified Castor Oil Incorporation on the Melt Processing and Physico-Chemical Properties of Polylactic Acid. *Polymers* **2022,** *14* (17), 3608.

46. Panaitescu, D. M.; Ionita, E. R.; Nicolae, C.-A.; Gabor, A. R.; Ionita, M. D.; Trusca, R.; Lixandru, B.-E.; Codita, I.; Dinescu, G., Poly (3-hydroxybutyrate) modified by

nanocellulose and plasma treatment for packaging applications. *Polymers* **2018,** *10* (11), 1249.

47. Panaitescu, D. M.; Frone, A. N.; Nicolae, C.-A.; Gabor, A. R.; Miu, D. M.; Soare, M.-G.; Vasile, B. S.; Lupescu, I., Poly (3-hydroxybutyrate) nanocomposites modified with even and odd chain length polyhydroxyalkanoates. *International Journal of Biological Macromolecules* **2023**, 125324.

48. Mottin, A. C.; Ayres, E.; Oréfice, R. L.; Câmara, J. J. D., What Changes in Poly(3-Hydroxybutyrate) (PHB) When Processed as Electrospun Nanofibers or Thermo-Compression Molded Film? *Materials Research* **2016,** *19*.

49. Majerczak, K.; Wadkin-Snaith, D.; Magueijo, V.; Mulheran, P.; Liggat, J.; Johnston, K., Polyhydroxybutyrate: a review of experimental and simulation studies of the effect of fillers on crystallinity and mechanical properties. *Polymer International* **2022,** *71* (12), 1398-1408. https://doi.org/10.1002/pi.6402.

50. El-Hadi, A.; Schnabel, R.; Straube, E.; Müller, G.; Henning, S., Correlation between degree of crystallinity, morphology, glass temperature, mechanical properties and biodegradation of poly (3-hydroxyalkanoate) PHAs and their blends. *Polymer testing* **2002,** *21* (6), 665-674.

51. Praveena, B.; Buradi, A.; Santhosh, N.; Vasu, V. K.; Hatgundi, J.; Huliya, D., Study on characterization of mechanical, thermal properties, machinability and biodegradability of natural fiber reinforced polymer composites and its Applications, recent developments and future potentials: A comprehensive review. *Materials Today: Proceedings* **2022,** *52*, 1255-1259.

52. Moreira, J. B.; Kuntzler, S. G.; da Silva Vaz, B.; da Silva, C. K.; Costa, J. A. V.; de Morais, M. G., Polyhydroxybutyrate (PHB)-based blends and composites. In *Biodegradable Polymers, Blends and Composites*, Elsevier: 2022; pp 389-413.

53. Kai, D.; Zhang, K.; Liow, S. S.; Loh, X. J., New Dual Functional PHB-Grafted Lignin Copolymer: Synthesis, Mechanical Properties, and Biocompatibility Studies. *ACS Applied Bio Materials* **2019,** *2* (1), 127-134. 10.1021/acsabm.8b00445.

54. Jandas, P. J.; Mohanty, S.; Nayak, S. K., Morphology and Thermal Properties of Renewable Resource-Based Polymer Blend Nanocomposites Influenced by a Reactive Compatibilizer. *ACS Sustainable Chemistry & Engineering* **2014,** *2* (3), 377-386. 10.1021/sc400395s.

55. Lapčík, L.; Maňas, D.; Lapčíková, B.; Vašina, M.; Staněk, M.; Čépe, K.; Vlček, J.; Waters, K. E.; Greenwood, R. W.; Rowson, N. A., Effect of filler particle shape on plastic-elastic mechanical behavior of high density poly(ethylene)/mica and poly(ethylene)/wollastonite composites. *Composites Part B: Engineering* **2018,** *141*, 92-99. https://doi.org/10.1016/j.compositesb.2017.12.035.

56. Fernández Armada, D.; González Rodríguez, V.; Costa, P.; Lanceros-Mendez, S.; Arias-Ferreiro, G.; Abad, M.-J.; Ares-Pernas, A., Polyethylene/ poly(3-hydroxybutyrate-co-3-hydroxyvalerate /carbon nanotube composites for eco-friendly electronic applications. *Polymer Testing* **2022,** *112*, 107642. https://doi.org/10.1016/j.polymertesting.2022.107642.

57. Wu, F.; Misra, M.; Mohanty, A. K., Challenges and new opportunities on barrier performance of biodegradable polymers for sustainable packaging. *Progress in Polymer Science* **2021,** *117*, 101395.

58. Jost, V.; Langowski, H.-C., Effect of different plasticisers on the mechanical and barrier properties of extruded cast PHBV films. *European Polymer Journal* **2015,** *68*, 302-312.

59. Meereboer, K. W.; Misra, M.; Mohanty, A. K., Review of recent advances in the biodegradability of polyhydroxyalkanoate (PHA) bioplastics and their composites. *Green Chemistry* **2020,** *22* (17), 5519-5558.

60. Muiruri, J. K.; Yeo, J. C. C.; Zhu, Q.; Ye, E.; Loh, X. J.; Li, Z., Poly (hydroxyalkanoates): production, applications and end-of-life strategies–life cycle assessment Nexus. *ACS Sustainable Chemistry & Engineering* **2022,** *10* (11), 3387-3406.

61. Niu, D.; Xu, P.; Liu, B.; Shao, H.; He, C.; Liu, T.; Yang, W.; Ma, P., Toward High Strength, Ductility, and Barrier Performance for Poly (glycolic acid)/Poly (butylene adipate-co-terephthalate) Green Films through Reactive Compatibilization and Biaxial Drawing. *Macromolecules* **2023**.

62. Parulekar, Y.; Mohanty, A. K.; Imam, S. H., Biodegradable nanocomposites from toughened polyhydroxybutyrate and titanate-modified montmorillonite clay. *Journal of nanoscience and nanotechnology* **2007,** *7* (10), 3580-3589.

63. Deokar, M. D.; Garnaik, B.; Sivaram, S., Toughening Poly(l-lactide) Blends: Effectiveness of Sequence-Controlled Six-Arm Star-Branched Block Copolymers of Poly(l-lactide) and Poly(ε-caprolactone). *ACS Omega* **2022,** *7* (11), 9118-9129. 10.1021/acsomega.1c04486.

64. Tsujimoto, T.; Haza, Y.; Yin, Y.; Uyama, H., Synthesis of branched poly (lactic acid) bearing a castor oil core and its plasticization effect on poly (lactic acid). *Polymer journal* **2011,** *43* (4), 425-430.

65. Lee, B.; Maher, M. J.; Schibur, H. J.; Hillmyer, M. A.; Bates, F. S., Toughening Polylactide with Graft-Block Polymers. *ACS Applied Polymer Materials* **2022,** *4* (5), 3408-3416. 10.1021/acsapm.2c00036.

66. Chen, H.; Oveissi, F.; Daly, S.; Shahrbabaki, Z.; Naficy, S.; Dehghani, F., A green and biodegradable plasticizer from copolymers of poly(β-hydroxybutyrate-co-ε-caprolactone). *Journal of Applied Polymer Science* **2022,** *139* (22), 52240. https://doi.org/10.1002/app.52240.

67. Muiruri, J. K.; Yeo, J. C. C.; Karen, T. Y.; Li, K.; Ye, E.; Loh, X. J.; Li, Z., Rapid dissolution of high concentration poly (3-hydroxybutyrate) using neoteric biosolvents: experiment and molecular dynamics simulation. *Green Chemistry* **2023,** *25* (13), 5276-5289.

68. Silva, M. R. P. d.; Matos, R. S.; Monteiro, M. D. S.; Santos, S. B.; Filho, H. D. F.; Andrade, G. R. S.; Salerno, M.; Almeida, L. E., Exploiting the Physicochemical and Antimicrobial Properties of PHB/PEG and PHB/PEG/ALG-e Blends Loaded with Ag Nanoparticles. *Materials* **2022,** *15* (21), 7544.

69. Melendez-Rodriguez, B.; Torres-Giner, S.; Lorini, L.; Valentino, F.; Sammon, C.; Cabedo, L.; Lagaron, J. M., Valorization of Municipal Biowaste into Electrospun Poly(3-hydroxybutyrate-co-3-hydroxyvalerate) Biopapers for Food Packaging Applications. *ACS Applied Bio Materials* **2020,** *3* (9), 6110-6123. 10.1021/acsabm.0c00698.

70. Wang, C.; Hsu, C.-H.; Hwang, I.-H., Scaling laws and internal structure for characterizing electrospun poly [(R)-3-hydroxybutyrate] fibers. *Polymer* **2008,** *49* (19), 4188-4195.

71. Quispe, M. M.; Lopez, O. V.; Boina, D. A.; Stumbé, J.-F.; Villar, M. A., Glycerol-based additives of poly(3-hydroxybutyrate) films. *Polymer Testing* **2021,** *93*, 107005. https://doi.org/10.1016/j.polymertesting.2020.107005.

72. Muiruri, J. K.; Liu, S.; Yeo, J. C. C.; Koh, J. J.; Kong, J.; Thitsartarn, W.; Teo, W. S.; He, C., Synergistic toughening of poly (lactic acid)–cellulose nanocrystal composites through cooperative effect of cavitation and crazing deformation mechanisms. *ACS Applied Polymer Materials* **2019,** *1* (3), 509-518.

73. Muiruri, J. K.; Liu, S.; Teo, W. S.; Kong, J.; He, C., Highly biodegradable and tough polylactic acid–cellulose nanocrystal composite. *ACS Sustainable Chemistry & Engineering* **2017,** *5* (5), 3929-3937.